PERFORMANCE ENHANCEMENT OF SOLAR STILL USING CONCENTRATED SOLAR RADIATION FROM POINT FOCUSING LENSES

Nibin T Koshy [a], V. Thirunavukkarasu[a]
[a] *Department of Mechanical Engineering, SRM Institute of Science and Technology, Kattankulathur, Chengalpattu, Tamil Nadu, India, 603203*

A R T I C L E I N F O

Keywords:
Modified solar still
Evaporation rate
Concentrated solar power
C o n v e x l e n s e s
ANSYS

A B S T R A C T

Globally it is estimated that two thirds of the population lives in a state of water scarcity for at least one month in a year and by 2050 over half the population is estimated to suffer from water scarcity. In order to combat against this future problem it is necessary to use the available saline water which constitutes about 97% of the available water on the earth's surface through desalination. Typical desalination processes are energy intensive and powered by fossil fuel consumption which makes it unaffordable for low and middle income nations. In such situations, solar stills can be seen as an effective way to mitigate the risks of water scarcity as solar stills have the advantage of not needing expensive fuel sources and skilled labour for carrying out its operations. The limitation of the typical still is that the production of water per hour is low and this can be attributed to the lower temperature gains in the saline water. The current research looks into the design, simulation and fabrication of an innovative solar still design which uses point focused radiation concentrated onto receiver tubes to enhance the operating temperature of the solar still. Thermal simulation is used to find the optimum material and dimensions for the receiver tube so as to achieve the maximum temperature and heat flux in the receiver tube of the design. The model is then fabricated and the temperature data is used to calculate the natural evaporation rate taking place within the model. The analysis software used in this study is ANSYS workbench version R2022. The study shows that receiver tube having minimum diameter, minimum thickness, and made of stainless steel is the optimum choice for the receiver in the solar still design and the increase in the operating temperature of the solar still results in the enhancement in the evaporation rates of the system..

1. Introduction

Water is an essential resource that sustains life and historically it is evident that all major civilizations set up their societies adjacent to water sources. In our modern world, it is a known fact that there is large scale urbanization taking place as more and more people seek to better their lives and the demand of water is expected to grow exponentially due to the increased demand on agriculture and industrial output.

Even though three quarter of the world is covered by water, over 97% of this water is saline water present in the oceans and the seas and less than 0.25% are available in easily accessible rivers and lakes. In order to meet this rising demand it is quintessential that there be cheaper and effective ways to carry out the desalination of saline water.

1.1. Background of desalination

The first commercial desalination plants began operation in the early 20th century with the first plant being established in Jedah, Saudi Arabia in 1907[1]. The middle east has been the global leader in establishing and operating desalination power plants, particularly due to the arid conditions and lack of freely available fresh water sources. Initially the majority of the plants were based on using thermal processes to heat the saline water, thereby vaporizing it. Later on, the multi stage flash process took precedence and was adopted by most of the gulf nations. The Office of Saline Water(OSW) established in the USA in the early 1950s carried out extensive research for nearly 3 decades up until 1979, spending over 1.5 billion US$ to develop membrane based technologies for desalination where saline water is pushed through a membrane under high pressure, which filters out the salinity in the water[10].

Based on the most recent report published by the IDA(International desalination association), globally there are over 21000 desalination plants that are active or under construction. It is estimated that the cumulative production of freshwater through desalination stood at 114.9 billion liters per day with the GCC nations housing over 9000 plants producing about 40 billion liters per day and presently nearly 1% of the world's freshwater comes through desalination methods[3] and although this is a small contribution, it is estimated that the global desalination capacity will double by the year 2030 due to the effects of changing climatic conditions and larger demand for freshwater combined with the expansion potential of desalination[4].

1.2 Groundwater resources

Due to the global rise in temperature, and weather changes that result in widespread droughts, the stress on the surface water is exasperated and this is resulting in societies depending on groundwater to fulfil the needs of its people. This has resulted in nearly half of the world population being dependent on groundwater sources, mostly for the purpose of irrigation[5].

While using groundwater, it is important to think of how that water got there and when it got there as water which has reached there within the last half-century has larger amounts of pollutant minerals and signatures of other man made chemicals while water from extracted from larger depths might also be contaminated with harmful pollutants like iron and manganese which require the use of expensive treatment to avoid health hazards[4]. Although at present the cost of procuring water is lower than that of producing desalinated water,

however, in the near future these may change due to the added cost of pumping water from deeper depths and the need for more expensive water treatment methods[6].

Considering this, it is important to think about sustainable and cost effective ways for the desalination of water.

1.3 Traditional desalination methods

The modern desalination plants are fossil fuel powered and release vast amounts of greenhouse gasses such as methane, nitrous oxide and CO_2 into the atmosphere. While the amount of these harmful gases released are dependent on the type of fuel used as well as the methodology and equipment used, generally it is estimated that a plant producing 1 million liters per day using thermal desalination would require 10000 tons of fuels each year[7] and using the reverse osmosis based desalination plants would release 0.4-6.7 tons of CO_2 for every million liters of desalinated water[8]. Globally it is estimated that 76 million tons of CO_2 has been emitted from fossil fuel powered desalination plants in the year 2020 and it is estimated that by 2040 the CO_2 emission could reach 218 million tons. Such large emissions drive climate change ultimately making them into climate catastrophes leaving large areas of the planet prone to severe drought while other areas are soaked due to excessive flooding.

All this clearly points to the fact that traditional desalination results in climate change which in turn results in an imbalance in the water reserves resulting in a need for more water to meet agricultural, industrial and domestic needs which ultimately leads back to the need for more desalination and if this demand is met with more traditional desalination, it then forms a viscous cycle that boosts itself resulting in unforeseeable consequences for humanity.

Another aspect of traditional water resources is the high energy costs associated with it and producing freshwater through desalination consumes large amounts of energy with the most energy efficient method of RO which by itself is 4 to 5 times more energy efficient than other thermal processes purification consumes about 8 to 10 times more energy than normal water treatment plants used for fresh water surface sources[9]. This clearly emphasizes the need for middle income and lower income nations which are not rich in fossil fuels to invest into the development of non fossil fuel based solar desalination processes.

1.4 Future desalination goals

It is evident that the future objectives of desalination(Fig. 1.1) must be to increase the use of clean green energy, with shared resources, recycling of brine combined with sustainable large-scale production and higher recovery models. The negative aspects of desalination processes that need to be minimized is the high energy consumption, environmental impact due to the brine byproduct and other chemicals used in the desalination process which negatively affects marine life if improperly released into the oceans as well as the high cost incurred due to the construction complexity of traditional desalination plants.

1.5 Desalination using solar stills

Solar still is a great device that meets most of the future goals of desalination processes as the device uses green energy by using the thermal energy from solar radiation. Traditional solar still are inexpensive to build due to their low construction complexity and does not require the need for skilled professionals to run the system. The conventional solar still used for desalination consists of a salt water basin covered by a transparent glass cover which is tilted at an angle that is close to the latitude of the location it is placed in. The incident solar radiation which transmits through the transparent cover impinges on the fluid, thereby heating the water and resulting water vapour being produced. The water vapour then condenses on the slopped cover from where it flows into a distillate channel under the action of gravity from where it is collected into a storage.

However, the conventional solar still has some drawbacks of not being able to have large scale productivity and several attempts have been made to enhance the output of the solar still by modifying the design of the solar still. Here, another such attempt is made to develop a design based on point focused radiation from convex lenses to enhance the thermal energy gained and thereby increase the productivity of the solar still by increasing the operation temperature which in turn increases the evaporation rate in the system.

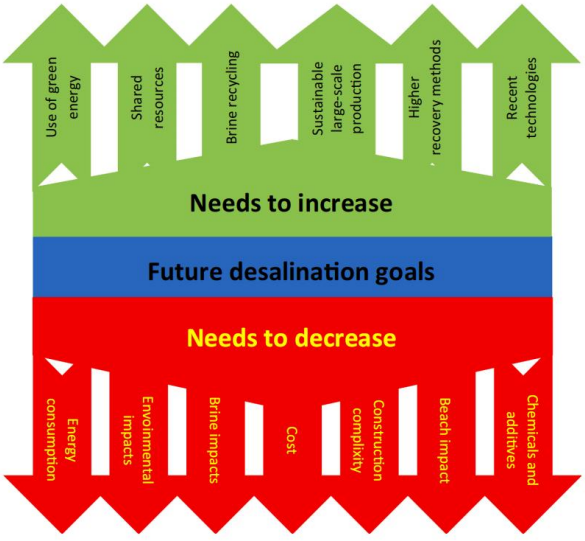

Fig 1.1. Future desalination goals to make desalination sustainable[4]

R_n	Net irradiance	T_a	Ambient temperature
ρ_a	Density of air	S_{spot}	Intensity of radiation at spot
C_p	Specific heat of air	$E_{focal\ point}$	Energy at focal point(W)
δe	vapor pressure deficit$[e_{s,a}(T_a)-e_a]$	$S_{incident}$	Intensity of incident solar radiation
g_a	momentum surface aerodynamic conductance	Δ	Slope of saturated vapour-pressure curve
λ_v	latent heat of vaporization of water	CSS	Conventional solar still
Υ	psychometric constant	MSS	Modified Solar still

2. Methods

The primary objective of this work is to investigate the effect of concentrated point focused radiation on the enhancement of the performance of the solar still by exposing a controlled volume of water in the still to a high intensity of solar radiation and measuring the enhancement in the evaporation rate.

In this report, the design of an innovative solar still is defined and the optimum parameters of the receiver tube such as the receiver tube thickness, receiver tube diameter and the receiver tube material are identified using transient thermal simulations. The transient thermal simulations are carried using the ANSYS software. The design of the system is based on the thermosyphon effect which deals with the natural convection of the fluid due to its higher temperature when compared to its surrounding temperature. The design is inspired by the knowledge gained from the literature survey and aims to enhance the evaporation rate which in turn results in higher distillation output and the overall effectiveness of the system. In order to achieve this, the design tries to reduce the volume of water subjected to solar radiation and minimize heat loses from the system.

3. Design and description

The design for the solar still is done in order to minimize the volume of water exposed to the solar radiation while allowing natural convection to move the water vapour from the still to the storage tank.

3.1. Computer aided design model

The proposed design of the solar still is as shown in below figures(Fig 3.1-3.3).

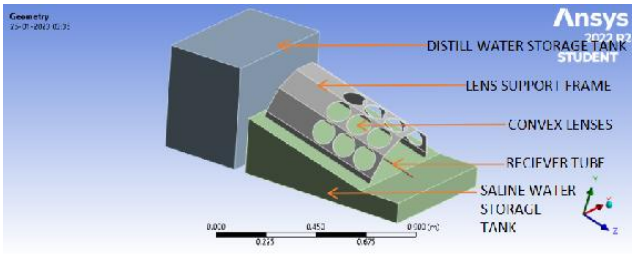

Fig 3.1. Isometric view of design

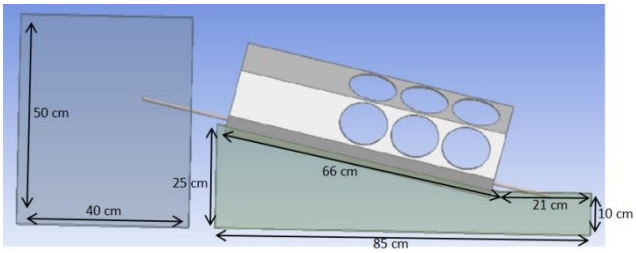

Fig 3.2. Side profile of design

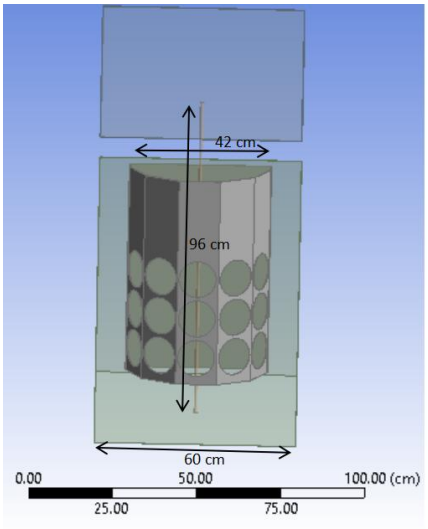

Fig 3.3. Top view of design

The design consists of a saline water storage tank, saline water channeling tube (receiver tube), lens support frame, convex lenses and a desalinated water storage tank. The descriptions for these components are further elaborated in this section.

3.2 Description of design components

- Saline water storage tank

The Saline water storage tank houses the poor quality water which needs to be treated. The design of the storage tank is similar to that of a conventional solar still as it consists of a sloped roof. The angle of inclination of the sloped roof is set to 13° as the local latitude in the region of Chennai is 13.0827°. This allows for the incident solar radiation to impinge perpendicularly on the design. The base of the storage tank is 85 cm in length with a height of 10

cm on the short side and a height of 25 cm on the taller end. The shorter end is extended from the slopped end of the top face to accommodate the inlet of the receiver tube.

- Saline water receiver tube

The saline water channeling tube is the receiver tube that absorbs the concentrated radiation from the point focusing lenses. The saline water from the storage tank enters the receiver tube from the inlet end of the tube and moves up through it by hydrostatic law to a level that matches the water level in the storage tank. The saline water in the receiver tube will absorb the energy absorbed by the receiver tube from the point focusing lenses and because of the lower thermal mass of the fluid inside the tube due to the smaller volume of water present in the tube, there will be a quicker rise in water temperature of the system which will result in critical temperature for evaporation happening sooner and thereby result in an enhancement of the distilled water output from the system. The water vapour generated in the receiver tube will rise due to the effects of buoyancy and move to the outlet of the receiver tube which is connected to the desalinated water storage tank.

- Convex lenses

The convex lenses used in the design are of 10 cm diameter and have been chosen as they are the largest lenses available at low cost and easy availability in the market. A total of 9 lenses are used in the design with 3 columns of lenses having 3 rows of lenses in each column. The lenses are arranged in rows keeping the convective nature of fluid flow in mind as this allows for the smaller volumes of fluid that absorbs the heat from the lower row of lenses to move up using buoyancy and is then further heated by the second row of lenses before being finally heated by the third row of lenses. In this way the heat loss that occurs due to convective flow of water to its surroundings is minimized.

- Lens support frame

The lens support frame is designed to house the convex lenses(Fig 3.3). The support frame is designed in such a way that it prevents the need for solar tracking mechanisms during the day. The design consists of 3 columns of support structure housing 3 rows of lenses in each column. The middle column of the lenses is parallel to the top surface of the of the storage tank while the columns on either side of the lenses are tilted at an angle of about 120° from the middle column. This is done to avoid complex solar tracking mechanisms and allow for the operation of the system throughout the day with minimum need of supervision. Each column of lens is at a distance of 10 cm from the receiver tube so that the receiver tube receives the highest intensity of solar radiation at all times. In addition to this, the lens support frame forms a sealed covering around the receiver tube which shields the receiver tube from ambient wind, thereby reducing the heat loss from the receiver tube to the surroundings. The support frame also makes use of diffused radiation by allowing incident solar radiation but preventing it reflected radiation from escaping using a principle similar to the green house effect.

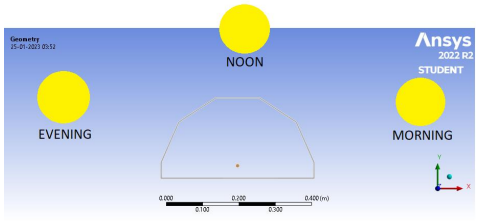

Fig 3.3. Front view of lens support frame

- Distilled water storage tank

The distilled water storage tank is used to condense and store the incoming steam from from the receiver tube. The distilled water storage tank is connected to the outlet of the receiver tube and also houses the condenser which converts the generated vapour into liquid water. This is expected to be done by passing the incoming stream of vapor through an enthalpy dissipating condenser like thick cotton or jute fibers through which the steam is passed in order to allow for the condensation of vapour.

4. Thermal Simulation

It is clear from the description of the design components that the receiver tube plays the most critical role in enhancing the performance of the solar still. The primary objectives of the thermal simulation is to understand the effects of thickness of the tube, diameter of the tube and the effects of material selection of the tube. In order to achieve this, a base case is selected and the output from the base case is compared to other cases and fundamental parameters like temperature and heat flux calculated by running the simulation is compared and their respective changes with relation to each others are compared.

The simulation is carried out be designing the geometry and adding some constant parameters of heat flow and convection loses to evaluate it. The simulation is carried out using ANSYS Workbench 2022 R2 using the transient thermal design module. The transient thermal module allows for the evaluation system to calculate the change in temperature and heat flux over a set amount of time. The parameters of the simulations are further described in the upcoming chapters.

4.1 Simulation assumptions

The assumptions made in carrying out the simulation are the following:

- Conductive heat transfer modelling with assumed convection loses.
- Internal convective flow of fluid is assumed to be negligible.
- Constant solar heat flux of 900 W/m2
- Radiation loses are assumed to be negligible.
- Concentration ratio of lens is 10:1

The simulation uses a conductive heat transfer modelling as the system is a passive system that does not use any external pumps to move the fluid through the inlet of the receiver and the fluid can be assumed to be stagnant through which the heat absorbed in the focal points of the lens at the receiver

moves through. This implies that the internal convective flow that is observed at the receiver tube is assumed to be negligible. Generally in fluids undergoing heating at one end, the volume of fluid that absorbs the thermal energy moves up due to the action of buoyancy while transferring heat to adjacent fluent particles through the action of conduction. The factors that affect this convective flow are several some of which are the fluids buoyancy, temperature, flow rate, shape and size of the passage and modelling this accurately requires more experimental data which does not fall into the purview of this research work.

A constant heat flux of 900 W/m^2 is assumed to be impinging on the surface as it allows for a more simplified model for comparison. The radiation loses from the system are assumed to be negligible as the system operating temperature is relatively low and the effects of radiation loses are more significant for systems operating at larger temperatures. The concentration ratio of the lens is set to 10:1 with the the lens focal point having a diameter of 10 mm.

4.2 Simulation parameter

- Ambient temperature = 22 °C
- Initial temperature of setup = 22 °C
- Area of lens = 78.5398 cm2
- Energy at focal point of lens = 7.068 Watts
- Intensity of solar radiation at focal point = 89992.57 W/m^2
- Convective heat loses from water to body = 20 W/m^2
- Convective heat loses from body to atmosphere = 4.3867 W/m^2

The ambient temperature of the surroundings in the system is set to be 22 °C and as a result the initial temperature of the setup is also the same. Each lens in the system has a radius of 10 cm the area of which is calculated using the following equation

$$A = \pi r^2 = \pi \times 5^2 = 78.5398 \text{ cm}^2$$

During any given time, only 1 column of the fixed lenses will be facing the sun and the energy at the focal point of the lens is given by the product of incident radiation to the area of each lens.

$$E_{\text{focal point}} = A \times S_{\text{incident}} = 78.5389 \times 10^{-4} \times 900 = 7.068 \text{ W}$$

The incident solar radiation is concentrated onto a spot at the focal point on the receiver tube. The intensity of solar radiation a the focal point given by the energy at the focal point divided by the area of the spot formed having a diameter of 1 cm.

$$S_{\text{spot}} = E_{\text{focal point}} \div A_{\text{spot}} = \frac{7.068}{\pi \times .0005^2} = 89992.57 \text{ W/m}^2$$

There are two types of convection loses that need to be accounted for in the system, with the first being the loses from the water in the receiver tube to the body and the second being the convection loses from the body to the surroundings. In the simulation the assumed convection loses from the receiver tube to the body is set as 20 W/m^2 and the loses from the body to the surroundings is set as 4.3867 W/m^2.

In order to carry out the comparative study, the transient thermal simulation is set to calculate the temperature and heat flux values over a duration of 10 minutes or 600 seconds(Fig 4.1).

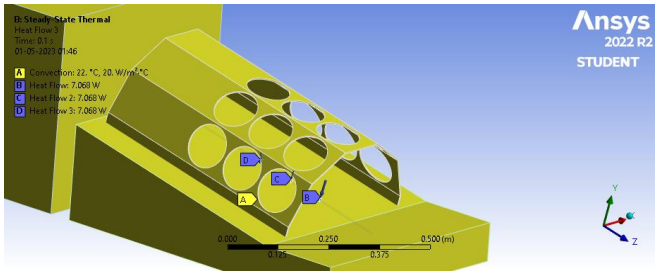

Fig 4.1: Simulated heat flow in system

4.3 Simulation base case

- Receiver tube inner diameter = 2 cm
- Receiver tube thickness = 1 mm
- Receiver tube material = Copper
- Thermal conductivity of copper = 400 W/m°C
- Specific heat of copper = 385 J/kg°C

As a base case to carry out the comparative study, the diameter of the inner tube is set to be 2 cm while the receiver tube thickness is set as 1 mm. The receiver tube material used in the base case is selected to be copper and this base case is compared with other cases in order to derive the optimal parameters of the receiver tube. The results from the simulation are described in the following figures.(Fig 4.2-4.3)

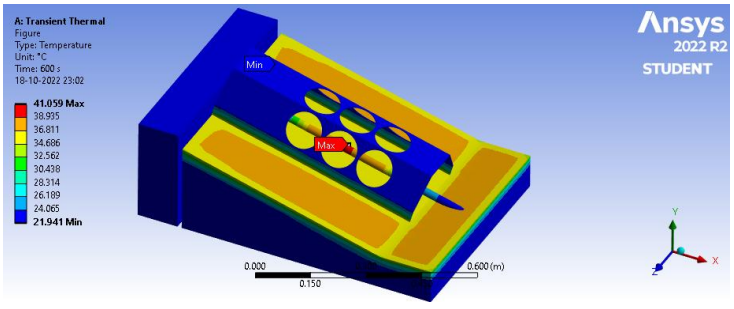

Fig 4.2. Temperature results for base case

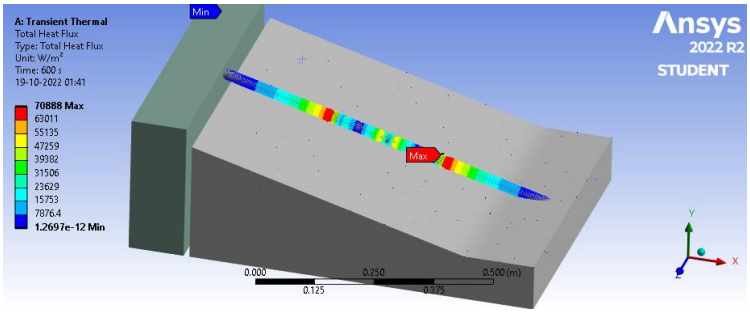

Fig 4.3. Heat flux values for base case

The maximum temperature observed in the system 41.059 °C at the focal point of the lens located in the middle row while the maximum heat flux in

the system is 70888 W/m^2 with the average heat flux observed in the system after the simulation time of 600 seconds found out to be 7848.5 W/m^2.

4.4 Variation of receiver tube diameter

Here, the simulation is carried out by varying the tube diameter of the receiver tube first to 1 cm to study the effects of decreasing the receiver tube diameter and the second to a diameter of 4 cm to study the effects of increasing the diameter of the receiver tube(Table 4.1).

Table 4.1:Effect of variation of receiver tube diameter in system

Inner Diameter (cm)	Max temperature (°C)		Max heat flux (W/m^2)		Average heat flux (W/m^2)	
2	41.059		70888		7848.5	
1	69.006	+68.06%	158420	+123.47%	20710	+163.87%
4	37.84	-7.83%	36343	-48.73%	4888.7	-37.71%

While varying the receiver tube diameter, it was seen that increasing the diameter would increase the cross sectional area and result in a larger volume of water being present in the receiver, requiring more volume of water being heated and hence, decreasing the diameter of the receiver tube significantly increases the maximum temperature and heat flux attained in the system.

4.5 Variation of receiver tube thickness

The receiver tube thickness is modified to understand the effects on maximum temperature and heat flux within system as the thickness of tube is varied. In the first case the thickness of the receiver tube is decrease to 0.5 mm while in the second case the thickness of the receiver tube is increased to 2 mm (Table 4.2).

Table 4.2: Effect of variation of thickness of receiver tube in system

Tube thickness (mm)	Max temperature (°C)		Max heat flux (W/m^2)		Average heat flux (W/m^2)	
1	41.059		70888		7848.5	
0.5	44.987	+9.56 %	124830	+76.09%	20585	+162.27%
2	37.851	-7.81%	69579	-1.84%	4759.4	-39.35%

It can also been seen that a reduction in the thickness reduces the thermal resistance of the tube which allows for more heat to be transferred to the water in the receiver tube. However due to the high thermal conductivity of copper used as receiver material in the base case, the heat accumulated is moved through the surface of the receiver tube and as a result the temperature gains in the system with a reduced thickness are moderate while the gains in heat flux of the system are high.

4.6 Variation of receiver tube material

The effects of variation of receiver tube material is simulated and the maximum temperature and heat flux observed is studied here. The various materials compared here are aluminium, cast iron and stainless steel. The specific heat and thermal conductivity of these materials are loaded from the Ansys thermal material library. The details of which are noted down in table 4.3.

Table 4.3: Thermal properties of simulated material

Material	Specific heat (J.kg^{-1}.°C^{-1})	Thermal conductivity (W.m^{-1}.°C^{-1})
Copper	385	400
Aluminium	951	237.5
Cast Iron	165	83
Stainless Steel	480	15.1

Table 4.4: Effect of variation of material of receiver tube in system

Receiver tube material	Max temperature (°C)		Average heat flux (W/m^2)	
Copper	41.059		7848.5	
Aluminium	44.266	+7.81%	6378.2	-18.73%
Cast iron	51.586	+25.63%	4477.6	-42.94%
Stainless steel	71.328	+73.72%	2551.8	-67.48%

There are two factors at play here which causes for an increase in the maximum temperature with a decrease in the heat flux when compared to the base case(Table 4.4). The first of these factors is the thermal conductivity of the material as a higher thermal conductivity results in the heat received in the system transferring the heat away from the focal point of the lens at the receiver surface throughout the body of the receiver faster than materials having lower thermal conductivity. In essence the materials having higher thermal conductivity acts as a heat spreader causing the heat to be quickly spread across the receiver surface and as a result the temperature rise in higher thermal conductivity materials like copper and aluminium is lower than that of materials like cast iron and stainless steel while the heat flux is larger in the case of copper and aluminium when compared to the other materials.

The second factor that affects the temperature rise in the system is the heat capacity of receiver tube with different materials. The heat capacity is the product of the materials specific heat and the mass of the receiver. It gives an idea about the amount of energy that needs to be absorbed by the receiver tube in order to raise the temperature of the tube by 1 °C and based on this concept, the cast iron tube will be able to raise its temperature at a faster rate while it will take longer for stainless steel to raise its temperature. However, as the thermal conductivity of stainless steel is significantly lower than that of cast iron, the rise in temperature of the stainless steel receiver is relatively higher than that of cast iron.

It is evident from the analysis of the results that the temperature and heat flux of the receiver tube are dependent on the tube diameter, tube thickness and the material selection of the tube.

5. Experimentation

The proposed model was fabricated after procuring the required materials from the local market and experimental work was carried out to find the operating temperature and evaporation rate of the system.

5.1 Fabrication

Fabrication was done by using acrylic sheets as the core material for building the saline water storage tank, the lens support frame and the desalinated water storage tank. Over 35 sq. ft. of 4 mm thick acrylic sheets were used for the fabrication of the setup. The sheets were bonded together using single component instant bonding adhesive METLOK 743. The setup was then sealed and made water proof by using silicone sealant to line the edges.

The fabrication of the storage tank was followed by the fabrication of the lens support frame. The lens support frame was made using 3 mm thick acrylic sheet to minimize the loss in solar radiation while travelling through the acrylic sheets. The design of the lens support frame is made in way to entrap the incoming solar radiation so that a large amount of the radiation may be absorbed by the receiver tubes. The lenses were then attached to each of the columns of the frame by using an adhesive glue.

During the fabrication, it was observed that the focal point of the sunlight is continuously moving and spending only a short time at the position where the tube was intended to be placed. In order to mitigate this issue, the position of the focal point of the sunlight impinging on the lenses in relation to the passage of time were experimentally tracked. The results from the experimental trails showed that most of the sunlight was focusing in a 20 cm space at a distance of 12 cm to 32 cm from the bottom corner of the lens support frame at a height of 1 cm or less.

The tracking of the focal point movement shows that at a time only 3 lenses from 1 column of the lens support frame focuses the sunlight within the structure and although all the focal points pass through the center, additional tubes were required to maximize the heat absorption. It was therefore decided to place an addition 3 steel tubes on either side of the receiver tube placed in the center making a total of 7 tubes(Fig 5.1).

The stainless steel tubes were of grade 304 and a thin cast iron sheet was placed below the steel tubes to further enhance heat absorption. The steel tubes and the cast iron sheet were painted matt black in colour to further enhance heat transfer. One end of the steel tubes were inserted into the saline water storage tank and sealed with M-Seal while the other end of the steel tubes were inserted into the distilled water storage tank.

Fig 5.1: 7 Steel tubes centrally inserted

5.2 Experimental setup

The final setup of the fabricated model is as seen in Fig 5.2.

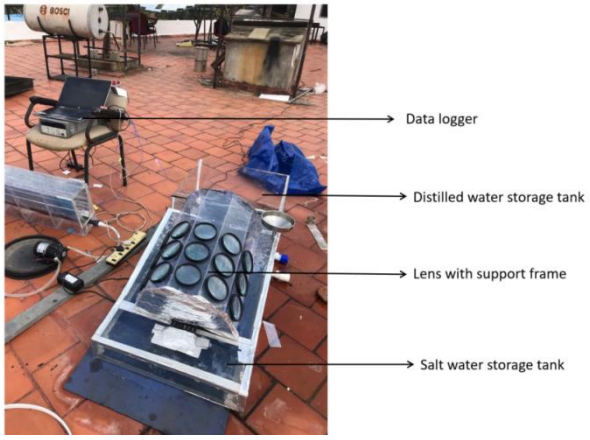

Fig 5.2: Experimental setup

In order to carry out the study, the salt water storage tank is filled with water so that the water may rise up from the bottom end of the steel tube to match the level of water in the tank. The grade of steel tube used for the experiment is SS 304, purchased from local steel merchants. The thermal properties of the steel are given in table 5.1 .

The lenses used in this setup were 15 numbers of double convex lenses of 10 cm diameter having a focal length of 20 cm. The specifications of the lenses are as given in the table 5.2 .

The temperatures on the surface of the receiver tube, and the temperature of the water within the tube were measured using j type thermocouples. The readings were saved using Keyence data logger .

The data was collected over several days over which there was minimal change in the overall temperature or performance of the solar still. The data for only one such day is presented here. The data collected on March 30th, 2023, in Chennai having a latitude of 13.08° and a longitude of 80.275° is presented in table 5.1.

The temperature data was collected using Keysight 34972A LXI Data Acquisition unit while the solar radiation data and ambient temperature were collected using GP2 advanced data logger and controller.

Table 5.1 :Thermal properties of stainless steel grade 304

Property	Value
Density	8000 kg/m^3
Melting point	1450 ℃
Modulus of Elasticity	193 GPa
Thermal Conductivity	16.2 W/m.K
Thermal Expansion	17.2 x 10^6 /K

Table 5.2: Convex lens specifications

Type	Double Convex lens
Colour	Clear
Material	Glass
Focal length	20 cm
Size	100 mm

5.3. Evaporation Rate calculation

The evaporation rate for stagnant water is primarily determined using the Penman model which has been validated by several research studies. The equation for the penman model is as given below[26].

$$E = \frac{\Delta R_n + \rho_a c_p \{e_{s,a}(T_a) - e_a\} k / r_a}{(\Delta + \gamma)\lambda} \quad (1)$$

Here, E is the evaporation rate while Δ is the slope of the saturation vapor pressure–temperature curve. R_n is the net radiation, while ρ_a is the air density, C_p is the specific heat, $e_{s,a}$(Ta) gives the vapor pressure of air at Ta ◦C and e_a gives the saturation pressure of air at Ta ◦C. Overall, it can be seen that the rate of evaporation is primarily a function of the vapour pressure and the amount of incident solar radiation with lesser effects due to the wind velocity. As the vapour pressure is directly dependent on the temperature of the water, the enhancement in the evaporation rate between a conventional solar still(CSS) which is at ambient temperature and the evaporation rate of the modified solar still(MSS) can be calculated and compared.

In order to calculate the evaporation rate, we first need to calculate the saturation pressure of water vapour at the ambient temperature and the temperature of the water inside the receiver tube. The equation to calculate this is obtained from a modified form of Clausius-Clapeyron equation[26], given by

$$e_{s,a}(T_a) = 0.61 exp\left(\frac{17.27 T_a}{T_a + 237.3}\right) \quad (2)$$

Multiplying the saturation vapour pressure with relative humidity gives the partial pressure of water vapor at that temperature.

$$e_a = \{RH \times e_{s,a}(T_a)\}/100 \quad (3)$$

Where T_a is the surface water temperature. In order to find the evaporation rate, we also need to calculate slope 'Δ' of the Saturated vapor pressure - temperature curve shown in figure .

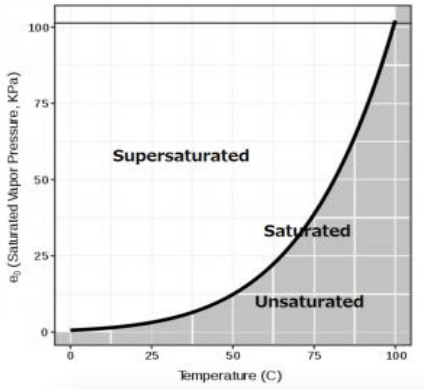

Fig 7.1: Saturation vapor pressure-temperature curve for water

The equation for calculating the slope is given by the following equation[26] .

$$\Delta = \frac{4098 e_{s,a}(T_a)}{(237.3 + T_a)^2} \quad (4)$$

Calculating the evaporation rate for the entire day and comparing the evaporation rate between the CSS and MSS produces table 5.2.

Table 5.1:Measured Data for 30th March 2023

Time	Surface Temp. ℃	Ambient Temp. ℃	Wind speed m/s	Total solar radiation W/m²	Diffused radiation W/m²	Beam radiation W/m²	Relative Humidity %
10:00	41.948	30	0.7	328	297	31	70
10:20	48.303	30.3	1.3	875	296	579	70
10:30	51.082	30.5	2.2	894	275	619	69
10:40	52.978	31	1.9	977	318	659	69
10:50	54.591	31.3	1.8	1056	398	658	68
11:00	57.807	31.6	1.4	907	309	598	67
11:10	54.406	31.8	1.4	971	405	566	66
11:20	56.872	31.8	1.8	1008	367	641	64
11:30	64.058	31.9	1.8	1058	364	694	63
11:40	55.409	32.3	0	1018	289	729	63
11:50	52.472	32.1	1.9	1017	304	713	63
12:00	58.099	32.6	1.9	505	374	131	63
12:10	61.79	32.7	1	1040	353	687	63
12:20	60.872	32.6	1.4	406	371	35	63
12:30	57.048	32.6	2.1	1041	320	721	63
12:40	59.179	33	1.9	946	300	646	63
12:50	58.645	33	2.4	842	305	537	63
13:00	59.502	33.5	2.6	1016	317	699	63
13:10	55.522	33.5	1.8	426	347	79	63
13:20	58.885	33.5	1.6	1034	361	673	63
13:30	61.088	34	2.1	1043	402	641	63
13:40	54.398	31.9	4.8	512	396	116	63
13:50	59.685	31.9	3.5	884	274	610	63
14:00	65.646	32	4.9	925	275	650	63
14:10	55.219	31.8	3.5	877	242	635	65
14:20	67.095	31.7	3.7	860	233	627	66
14:30	61.595	31.6	5.1	830	227	603	67
14:40	59.518	31.5	5.6	801	234	567	67
14:50	57.823	31.5	4.9	764	231	533	66
15:00	56.642	31.5	3.7	743	217	526	66
15:10	55.057	31.2	4.6	710	209	501	64
15:20	53.233	31.1	3.5	678	190	488	64
15:30	52.746	30.8	4.8	643	179	464	63
15:40	52.008	30.8	4	599	170	429	63
15:50	52.614	30.6	2.4	552	162	390	64
16:00	58.32	30.5	4.6	520	151	369	65
16:10	53.244	30.3	5.1	477	145	332	67
16:20	49.095	30.1	4.8	431	139	292	69
16:30	43.469	30.1	3.3	388	131	257	70
16:40	49.05	29.9	3.7	350	121	229	70
16:50	46.79	29.9	2.7	307	110	197	70
17:00	46.607	29.9	2.4	283	109	174	70

Table 5.2: Evaporation rate of CSS and MSS

Time	Surface Temp. ℃	Internal Temp. ℃	Ambient Temp. ℃	Total solar radiation W/m^2	E_{CSS} Kg s^{-1} m^{-2}	E_{MSS} Kg s^{-1} m^{-2}	Change %
10:00	41.948	40.634	30	328	1.4396E-04	1.6153E-04	12.21
10:10	44.625	43.757	30.5	894	3.0993E-04	3.5041E-04	13.06
10:20	48.303	46.444	30.3	875	3.1987E-04	3.6782E-04	14.99
10:30	51.082	47.873	30.5	894	3.2805E-04	3.7962E-04	15.72
10:40	52.978	51.799	31	977	3.5679E-04	4.1863E-04	17.33
10:50	54.591	54.69	31.3	1056	3.8495E-04	4.5591E-04	18.43
11:00	57.807	55.675	31.6	907	3.3916E-04	4.0348E-04	18.96
11:10	54.406	53.634	31.8	971	3.6212E-04	4.2552E-04	17.51
11:20	56.872	53.967	31.8	1008	3.7687E-04	4.4371E-04	17.73
11:30	64.058	53.391	31.9	1058	3.9494E-04	4.6303E-04	17.24
11:40	55.409	53.895	32.3	1018	3.8360E-04	4.4913E-04	17.08
11:50	52.472	50.668	32.1	1017	3.8243E-04	4.4160E-04	15.47
12:00	58.099	57.045	32.6	505	2.1642E-04	2.6097E-04	20.59
12:10	61.79	61.138	32.7	1040	3.9251E-04	4.7135E-04	20.09
12:20	60.872	59.733	32.6	406	1.8391E-04	2.2653E-04	23.17
12:30	57.048	54.673	32.6	1041	3.9241E-04	4.5940E-04	17.07
12:40	59.179	54.152	33	946	3.6278E-04	4.2264E-04	16.50
12:50	58.645	53.68	33	842	3.2850E-04	3.8271E-04	16.50
13:00	59.502	55.189	33.5	1016	3.8790E-04	4.5105E-04	16.28
13:10	55.522	53.081	33.5	426	1.9248E-04	2.2601E-04	17.42
13:20	58.885	54.401	33.5	1034	3.9386E-04	4.5620E-04	15.83
13:30	61.088	56.941	34	1043	3.9889E-04	4.6475E-04	16.51
13:40	54.398	52.523	31.9	512	2.1692E-04	2.5736E-04	18.64
13:50	59.685	56.648	31.9	884	3.3821E-04	4.0396E-04	19.44
14:00	65.646	61.761	32	925	3.5198E-04	4.2822E-04	21.66
14:10	55.219	50.479	31.8	877	3.3285E-04	3.8585E-04	15.92
14:20	67.095	59.502	31.7	860	3.2560E-04	3.9391E-04	20.98
14:30	61.595	60.486	31.6	830	3.1413E-04	3.8200E-04	21.61
14:40	59.518	56.513	31.5	801	3.0436E-04	3.6483E-04	19.87
14:50	57.823	52.775	31.5	764	2.9369E-04	3.4646E-04	17.97
15:00	56.642	52.277	31.5	743	2.8687E-04	3.3775E-04	17.74
15:10	55.057	51.823	31.2	710	2.7785E-04	3.2822E-04	18.13
15:20	53.233	51.556	31.1	678	2.6718E-04	3.1586E-04	18.22
15:30	52.746	51.843	30.8	643	2.5626E-04	3.0511E-04	19.06
15:40	52.008	50.062	30.8	599	2.4208E-04	2.8578E-04	18.05
15:50	52.614	48.269	30.6	552	2.2505E-04	2.6373E-04	17.19
16:00	58.32	47.707	30.5	520	2.1317E-04	2.4939E-04	16.99
16:10	53.244	46.699	30.3	477	1.9622E-04	2.2874E-04	16.57
16:20	49.095	48.807	30.1	431	1.7840E-04	2.1159E-04	18.61
16:30	43.469	42.235	30.1	388	1.6334E-04	1.8504E-04	13.29
16:40	49.05	46.611	29.9	350	1.5079E-04	1.7743E-04	17.67
16:50	46.79	44.722	29.9	307	1.3706E-04	1.5951E-04	16.38

6. Results and Discussion

It is evident from the calculated evaporation rate that the performance of the MSS is better than the performance of CSS and this can be attributed to the fact that the higher temperature in the MSS results in a higher evaporation rate. The temperature profile chart for the setup is given in figure 6.1.

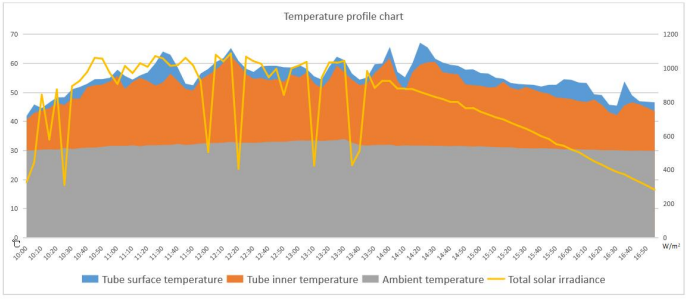

Fig 6.1: Temperature profile chart

The temperature profile chart shows the ambient temperature with respect to the water temperature given by the tube inner temperature and the surface temperature of the tube. It can be seen from the profile that the surface temperature of the tube is the highest while that of the water is sightly lower, this is due to the fact that the sunlight directly impinges on the receiver tube from where the heat is absorbed into the water. As the receiver tube is only 1 mm thick, the heat absorbed by the receiver tube is easily absorbed into the water as the low thermal conductivity of the steel tubes prevents the heat from quickly spreading through the surface of the tube and enhances the heat absorption into the water. It is evident that the receiver tube is able to maintain the water at much higher temperature than ambient and thereby enhance the evaporation rate.

Another observation is that a reduction in the solar radiation due to cloud cover does not significantly affect the ambient temperature but reduces the surface temperature of the receiver tube which in turn reduces the water temperature.

The comparison between the evaporation rate of the CSS and MSS is presented in the figure 6.2.

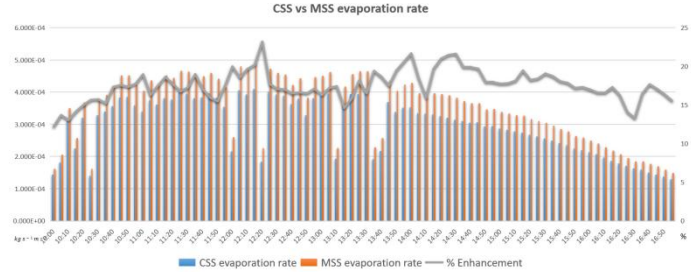

Fig 6.2: Comparison of evaporation rate between CSS and MSS

It is evident from the above comparison that the evaporation rate of the MSS is higher than that of the CSS with a peak efficiency over 20 % obtained during noon while the lowest efficiency was obtained during early morning and evening where the surface temperature is the lowest.

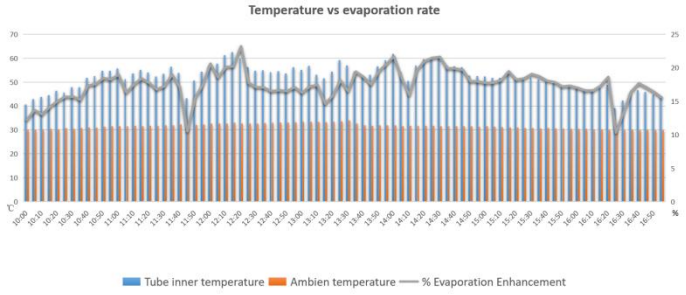

Fig 6.3: Effect of temperature on evaporation rate

By comparing the temperature values of the water with the temperature of the ambient(Fig 6.3), it is evident that the larger the temperature difference between the ambient and the receiver tube, the higher is the enhancement in evaporation rate of the solar still.

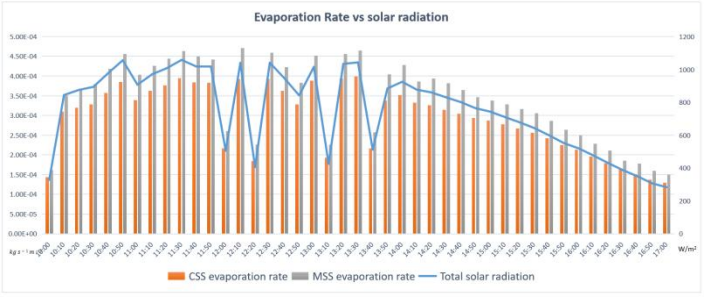

Fig 6.4: Effect of solar radiation on evaporation rate

When comparing the evaporation rate with the amount of incident solar radiation(Fig 6.4), it is evident that a reduction in the solar radiation significantly reduces the amount of evaporation while an enhancement in solar radiation increases the amount of evaporation. This can be attributed to the fact that evaporation is a surface phenomenon and occurs due to the particles close to the surface absorbing the energy from the solar radiation and escaping in the form of vapors from the bulk volume of the fluid.

It can therefore be seen that the performance of a solar still can be enhanced by using concentrated solar radiation from point focusing lenses. The point focusing lenses and the lens support frame trap the incoming solar radiation which absorbs heat into the receiver tube containing water, the small amount of water present inside the tube absorbs the heat and transforms into water vapour at faster rate when compared to a conventional solar still. The water vapour then moves up the tube and is collected in the desalinated water storage tank.

7. Conclusion

Based on the transient thermal simulation carried out using the Ansys software, the design and fabrication of the solar still using point focusing

concentrated solar radiation was carried out and the enhancement in the operating temperature was measured .

The following conclusions can be drawn from the work.

- The receiver tube diameter and thickness needs to be as low as possible, for maximum temperature gains.
- Lower thermal conductivity and heat capacity allows for higher temperature gains in the receiver tube by concentrating the thermal energy in a few bands.
- The modified solar still operates at a higher temperature and gave 12.5% to 23% enhancement in the evaporation rate when compared to a conventional solar still operating at the ambient temperature.
- Higher temperature difference from the ambient temperature and higher radiation levels results in a higher evaporation rate.

References

[1] D. Curto, V. Franzitta, A. Guercio, A review of the water desalination technologies, Appl. Sci. 11 (2) (2021) 670.

[2].Mekonnen, Mesfin M.; Hoekstra, Arjen Y. (2016). "Four billion people facing severe water scarcity". Science Water Stress Advances. doi:10.1126/sciadv.1500323. ISSN 2375-2548.

[3] J. Eke, A. Yusuf, A. Giwa, A. Sodiq, The global status of desalination: an assessment of current desalination technologies, plants and capacity, Desalination 495 (2020), 114633.

[4]Muhammad Ayaz , M.A. Namazi , M. Ammad ud Din , M.I. Mohamed Ershath , Ali Mansour , el-Hadi M. Aggoune , Sustainable seawater desalination: Current status, environmental implications and future expectations, Desalination 540 (2022) 116022

[5] P. D¨oll, et al., Impact of water withdrawals from groundwater and surface water on continental water storage variations, J. Geodyn. 59 (2012) 143–156.

[6] A. Pistocchi, et al., Can seawater desalination be a win-win fix to our water cycle? ,Water Res. 182 (2020), 115906.

[7] A. Tal, Addressing desalination's carbon footprint: the israeli experience, Water 10 (2) (2018) 197.

[8] K. Cornejo, M.V. Santana, D.R. Hokanson, J.R. Mihelcic, Q. Zhang, Carbon footprint of water reuse and desalination: a review of greenhouse gas emissions and estimation tools, J. Water Reuse Desalin. 4 (4) (2014) 238–252.

[9] Voutchkov, Energy use for membrane seawater desalination–current status and trends, Desalination 431 (2018) 2–14.

[10] Desalination: an ocean of problems. https://foodandwaterwatch.org/wp-content /uploads/2021/03/desalination_fs_oct_2009.pdf?fbclid=IwAR1ymAFxfJw2uCs R0ZOxR4fghRgRe-kk7KHL3nUoUrijvXBP-9R6sxvvBi8

[11] Emad Ghandourah, Hitesh Panchal , Othman Fallatah, Haitham M. Ahmed, Essam B.Moustafa, Ammar H. Elsheikh, Performance enhancement and economic analysis of pyramid solar still with corrugated absorber plate and conventional solar still: A case study Case Studies in Thermal Engineering 35 (2022) 101966, https://doi.org/10.1016/j.csite.2022.101966

[12] F.A. Essa, Wissam H. Alawee, Suha A. Mohammed, Hayder A. Dhahad, A. S. Abdullah , Z.M. Omara ,Experimental investigation of convex tubular solar still performance using wick and nanocomposites, Case Studies in Thermal Engineering 27 (2021) 101368, https://doi.org/10.1016/j.csite.2021.101368

[13] F.A. Essa, A.S. Abdullah, Wissam H. Alawee, A. Alarjani, Umar F. Alqsair, S.Shanmugan, Z.M. Omara, M.M. Younes,Experimental enhancement of tubular solar still performance using rotating cylinder, nanoparticles' coating, parabolic solar concentrator, and phase change material, Case Studies in Thermal Engineering 29 (2022) 101705, https://doi.org/10.1016/j.csite.2021.101705

[14] Akram H. Abed, Hisham Assi Hoshi, Mohammed Hassan Jabal, Experimental investigation of modified solar still coupled with high-frequency ultrasonic vaporizer and phase change material capsules, Case Studies in Thermal Engineering 28 (2021) 101531, https://doi.org/10.1016/j.csite.2021.101531

[15] Chemseddine Maatki, Heat transfer enhancement using CNT-water nanofluids and two stages of seawater supply in the triangular solar still, Case Studies in Thermal Engineering 30 (2022) 101753, https://doi.org/10.1016/j.csite.2021.101753

[16] Mohammad Hemmat Esfe, Davood Toghraie, Numerical study on the effect of solar radiation intensity on the fresh water productivity of solar still equipped with Thermoelectric Cooling System (TEC) for hot and dry areas of Semnan, Case Studies in Thermal Engineering 32 (2022) 101848,https://doi.org/10.1016/j.csite.2022.101848

[17] S.S. Tuly, M.S. Islam, Rakibul Hassan, Barun K. Das, M.R.I. Sarker, Investigation of a modified double slope solar still integrated with nanoparticle-mixed phase change materials: Energy, exergy, exergo-economic, environmental, and sustainability analyses, Case Studies in Thermal Engineering 37 (2022) 102256, https://doi.org/10.1016/j.csite.2022.102256

[18] Abdulmohsen O. Alsaiari, S. Shanmugan, Hani Abulkhair, Ahmad Bamasag, Essam B. Moustafa, Radi A. Alsulami, Iqbal Ahmad, Ammar Elsheikh, Applications of TiO2/Jackfruit peel nanocomposites in solar still: Experimental analysis and performance evaluation, Case Studies in Thermal Engineering 38 (2022) 102292, https://doi.org/10.1016/j.csite.2022.102292

[19] Mohamed M.Z. Ahmed, Fuhaid Alshammari, Umar F. Alqsair, Muapper Alhadri, A.S. Abdullah, Mohamed Elashmawy, Experimental study on the effect of the black wick on tubular solar still performance, Case Studies in Thermal Engineering 38 (2022) 102333, https://doi.org/10.1016/j.csite.2022.102333

[20] Jyotin Kateshia , Vikas Lakhera, A comparative study of various fatty acids as phase change material to enhance the freshwater productivity of solar still, Journal of Energy Storage 48 (2022) 103947, https://doi.org/10.1016/j.est.2021.103947

[21] Hitesh N Panchal, Dr. P. K. Shah, Effect of Varying Glass cover thickness on Performance of Solar still: in a Winter Climate Conditions, International Journal Of Renewable Energy Research, IJRER, Vol.1, No.4, pp.212-223 ,2011

[22] Seyed Sina Adibi Toosi, Hamid Reza Goshayeshi, Saeed Zeinali Heris, Experimental investigation of stepped solar still with phase change material and external condenser, Journal of Energy Storage 40 (2021) 102681, https://doi.org/10.1016/j.est.2021.102681

[23] M.M. Younes, A.S. Abdullah, F.A. Essa, Z.M. Omara, Half barrel and corrugated wick solar stills – Comprehensive study, Journal of Energy Storage 42 (2021) 103117, https://doi.org/10.1016/j.est.2021.103117

[24] A.S. Abdullah, Z.M. Omara, Habib Ben Bacha, M.M. Younes, Employing convex shape absorber for enhancing the performance of solar still desalination system, Journal of Energy Storage 47 (2022) 103573, https://doi.org/10.1016/j.est.2021.103573

[25] H.L. Penman, Natural evaporation from open water, bare soil and grass, Proc. R. Soc. Lond. 193 (1948) 120–145, https://doi.org/10.1098/rspa.1948.0037

[26] Min Sik Kim, Dongwon Cha , Se Mi Lee , Hyungjin Jeong , Changha Lee, Prediction of brine evaporation rate in a pond: Development of different models under controlled meteorological conditions and comparative evaluation, Desalination 551 (2023) 116415, https://doi.org/10.1016/j.desal.2023.116415